Chemical Engineering Journal 379 (2020) 122268

Contents lists available at ScienceDirect

Chemical Engineering Journal

journal homepage: www.elsevier.com/locate/cej

A polymer nanocomposite coating with enhanced hydrophilicity, antibacterial and antibiofouling properties: Role of polymerizable emulsifier/anionic ligand

Yu Chen, Yong Ding, Junping Zheng*

School of Materials Science and Engineering, and Tianjin Key Laboratory of Composite and Functional Materials, Tianjin University, Tianjin 300350, China

HIGHLIGHTS

- Ag NPs were evenly dispersed to 5 nm by electrostatic interaction with ligand SMDM.
- Polymer nanocomposite coatings were prepared by SMDM as polymerizable emulsifier.
- The coating exhibited greatly improved hydrophilicity and wettability.
- The coating showed excellent and long-term antibacterial and antibiofouling ability.
- A green, simple and universal reference for the uniform dispersion of nanoparticles.

ARTICLE INFO

Keywords:
Polymer nanocomposite
Anionic ligand
Polymerizable emulsifier
Dispersion
Antibacterial/antibiofouling coating

ABSTRACT

Considerable attention has been devoted to producing polymer/Ag nanocomposite antibacterial coatings. However, agglomeration problems of Ag nanoparticles (Ag NPs) and complex preparation process greatly limit their performance and applications. This study reports a green, efficient, convenient and universal strategy for the preparation of antibacterial polyacrylate/Ag nanocomposite coatings via emulsion polymerization. In this work, a new type of polymerizable emulsifier, sodium mono dodecyl maleate (SMDM) was successfully synthesized, which also acted as an anionic ligand to achieve the uniform dispersion of Ag NPs in the polymer matrix by electrostatic interaction with Ag NPs. X-ray diffraction indicated that Ag NPs were successfully introduced into the coatings. Meanwhile, the results of transmission electron microscopy and scanning electron microscope demonstrated that Ag NPs were uniformly dispersed in the polymer matrix due to the action of SMDM, and the particle sizes were reduced to about 5 nm. Furthermore, the systematic investigations into the surface properties and antibacterial properties indicated that the nanocomposite coatings displayed greatly improved hydrophilicity, wettability, excellent antibacterial and antibiofouling ability. In a short period of time, the nanocomposite coatings could approach or even reach the superhydrophilic state. Besides, the nanocomposite coatings maintained close to 100% antibacterial rate and completely inhibited bacterial adhesion and biofilm formation in 7 days. It is believed that this approach has great potential to be applied in various fields where antibacterial properties are highly demanded and this method is expected to provide a promising reference for the uniform dispersion of other nanoparticles and the preparation of different functionalized coating materials.

1. Introduction

Microbial infections and pollution have become an increasingly serious problem, which greatly affects the quality and longevity of industrial products, and in turn adversely affects human health and safety [1–3]. Due to outstanding comprehensive properties, polymer coatings have a wide range of applications, such as the automotive industry, medical, home appliances, construction, packaging and so on [4–6]. However, further development of polymer coatings has been limited because of bacterial contamination and fouling. In order to solve this problem, it is a versatile and effective method to introduce antibacterial agents into polymer coatings to prepare composite coatings [7,8]. Antibacterial agents mainly include inorganic antibacterial agents, organic antibacterial agents and natural antibacterial agents [9,10].

* Corresponding author.
E-mail address: jpzheng@tju.edu.cn (J. Zheng).

https://doi.org/10.1016/j.cej.2019.122268
Received 9 April 2019; Received in revised form 1 June 2019; Accepted 16 July 2019
Available online 17 July 2019
1385-8947/

Unfortunately, organic antibacterial agents [11–15] and natural antibacterial agents [16–18] have some insurmountable defects and limitations. Among all antibacterial agents, Ag nanoparticles (Ag NPs) have unparalleled advantages, such as superior bactericidal performance, broad antimicrobial spectrum, high stability, remarkably low human toxicity and no drug resistance [19–21]. Moreover, compared with Ag^+, Ag NPs have more stable physicochemical properties and lower effective antibacterial concentration (Ag NPs are nanomolar and Ag^+ is micromolar) [22,23]. In addition, due to its extremely small particle size and high specific surface area, Ag NPs can easily enter bacteria and have a large contact area with bacteria. Therefore, it is a practical, effective and promising method to introduce Ag NPs into polymer coatings to endow them with antibacterial properties.

Studies have shown that the antibacterial effect of Ag NPs has an important relationship with the particle size: the smaller the particle size, the better the antibacterial effect [24–27]. However, Ag NPs tend to agglomerate and are difficult to disperse uniformly, which seriously weakens the antibacterial effect. Some methods have been adopted to deal with the intractability problem. One of the most common methods is to add a strong reducing agent to reduce Ag^+, such as $AgNO_3$, and generate Ag NPs in situ, thereby preventing aggregation of Ag NPs to some extent [25,28,29]. However, this method is prone to result in more complicated preparation process and also brings potential risks to the environment. More importantly, reducing agents and other materials such as stabilizers used during the synthesis of Ag NPs can leave chemical debris and impurities on the materials, which has negative impacts on the size and performance of Ag NPs [30]. Another widely used method is surface modification of Ag NPs to improve the dispersion [31–33]. Nevertheless, most methods of surface modification that have been reported so far are complicated in operation and cumbersome in steps, incur additional costs, have a negative impact on the environment, and even impair the overall performance of products, which are hurdles to large-scale production and commercialization. In addition, some other ways have also been employed to evenly disperse Ag NPs, however they all have certain limitations [34–36]. In fact, most of the methods currently used fail to achieve truly complete uniform dispersion of Ag NPs. Therefore, a better and greener method urgently needs to be adopted to uniformly disperse Ag NPs in polymer matrices. Studies have demonstrated that in the aqueous medium, the surface of nanoparticles exhibits positive or negative potentials owing to their unique surface characteristics [37,38]. Based on this, it is a potential and feasible method to design suitable ionic organic ligands and achieve uniform dispersion of Ag NPs via electrostatic interaction.

Emulsion polymerization is widely used in the preparation of polymer nanocomposite coatings. At the same time, studies have shown that emulsion polymerization is also an effective way to uniformly disperse nanoparticles in a polymer matrix [39]. Therefore, the use of emulsion polymerization provides a valid way for the uniform dispersion of Ag NPs and the preparation of antibacterial coatings. However, traditional emulsifiers that remain in the products adversely affect the performance of the products and cause damage to the environment. Compared with traditional emulsifiers, the introduction of polymerizable emulsifiers [40,41] is a practical and meaningful solution to this problem, which can copolymerize with the main monomers and avoid the deficiency of traditional emulsifiers.

In this work, we proposed a novel, simple, effective and eco-friendly strategy to prepare polyacrylate/Ag nanocomposite antibacterial coating with excellent performance. Commercial Ag NPs were used and a polymerizable emulsifier sodium mono dodecyl maleate (SMDM) was synthesized, which also acted as an anionic ligand, interacting with the charge on the surface of Ag NPs and allowing Ag NPs to be uniformly dispersed in the polymer matrix. Through our method, Ag NPs were successfully introduced into the polymer matrix and achieved extremely uniform dispersion, which the particle sizes were reduced to about 5 nm. The prepared nanocomposite coatings exhibited excellent antibacterial and antibiofouling activity against both Gram-negative bacteria (*E. coil*) and Gram-positive bacteria (*S. aureus*) as well as improved mechanical properties, hydrophilicity and wettability thanks to the uniform dispersion of Ag NPs. This method is expected to provide a promising approach for the uniform dispersion of a variety of nanoparticles and the preparation of functionalized nanocomposite coating materials.

2. Experiment

2.1. Materials

Ag NPs (60–120 nm, 99.5 wt%) were purchased from Shanghai Macklin Biochemical Technology Co., Ltd. 4-Vinylbenzyl chloride (analytical grade) and 1-Dodecanamine (analytical grade) were purchased from Tianjin Heowns Biochemical Technology Co., Ltd. Maleic anhydride (analytical grade) and Dodecyl alcohol (analytical grade) were purchased from Tianjin Jiangtian Chemical Technology Co., Ltd. Potassium persulfate (KPS, analytical grade, Tianjin Yuanli Chemical Co., Ltd) was used as initiator. Methyl methacrylate (MMA) was procured from Tianjin Yuanli Chemical Co., Ltd and Butyl acrylate (BA) was procured from Tianjin Damao Chemical Reagent Factory. Sodium dodecyl sulfate (SDS, analytical grade) and Heptane (analytical grade) were purchased from Tianjin Jiangtian Chemical Technology Co., Ltd. Other reagents were all of analytical grade. Deionized water was used throughout.

2.2. Synthesis of SMDM

SMDM was synthesized as below. Maleic anhydride and 1-dodecanol were stirred and heated to 60 °C to melt completely, followed by reaction at 80 °C for 1 h. Then, heptane was added to the reaction mixture, which was stirred to homogeneous and transparent liquid. After that, the solution was stirred at room temperature for 3 h and then at 15 °C for 2 h. The precipitate that formed was collected and recrystallized from heptane. Then the obtained white crystals melted in acetone at 60 °C and 40% NaOH aqueous solution was dropwise added with rapid stir. After cooling, the white solid was obtained by suction filtration and precipitate was collected and dried under vacuum. The product was a white powder. The characterization results of SMDM are shown in Fig. S2, which exhibits SMDM was successfully synthesized.

2.3. Preparation of nanocomposite emulsions

The mixture of deionized water, 0.5 g SMDM, 0.057 g KPS, MMA and BA (mass ratio was 1:1) was pre-emulsified for 2.5 h under stirring at 700 rpm. After 2.5 h, the pre-emulsion was poured in constant pressure funnel for future use. The ultrasonic dispersion of Ag NPs was performed immediately after the pre-emulsification was started. The mixture of deionized water, Ag NPs (2.50 wt%, based on monomers mass, the same below) and 0.5 g SMDM was sonicated for 30 min to preliminarily achieve uniform dispersion. The ultrasonically dispersed mixture with MMA and BA (mass ratio was 1:1) were pre-emulsified for 30 min under stirring at 700 rpm. Next, the reaction system was heated to 70 °C, followed by 0.057 g KPS. Then, the system was heated to 75 °C and reacted for 30 min. 30 min later, the pre-emulsion was dropwise added in the system in 1 h. After that, the system was heated to 82 °C and sequentially polymerized for another 2 h for sufficient reaction. After the reaction, the prepared latex was washed, filtered and centrifuged to obtain pure products, named P(MMA-co-BA-co-SMDM)/$Ag_{2.50}$.

In order to study the effect of different Ag NPs content on the coating properties and obtain the best comprehensive performance, 1.25 wt% and 3.75 wt% Ag NPs were also selected to prepare nanocomposite emulsions according to the same preparation process as above, and the products were named as P(MMA-co-BA-co-SMDM)/$Ag_{1.25}$ and P(MMA-co-BA-co-SMDM)/$Ag_{3.75}$, respectively.

To verify the effect of SMDM as polymerizable emulsifier and its superior performance in dispersing Ag NPs and preparing nanocomposite emulsions, the traditional emulsifier SDS instead of SMDM was used to prepare nanocomposite emulsions, and the preparation method was the same as above and Ag NPs were added in an amount of 2.50 wt%, which the products were named P(MMA-co-BA)/SDS/$Ag_{2.50}$.

Pure polymer matrix was also prepared, named P(MMA-co-BA).

2.4. Preparation of nanocomposite coatings

Nanocomposite coatings were prepared by casting. Specifically, coatings were cast from the emulsions as mentioned above, which were uniformly cast onto Teflon molds, and were first dried at room temperature for 48 h and then dried under vacuum at 50 °C for 48 h to thoroughly remove moisture.

2.5. Characterizations

The ^{1}H nuclear magnetic resonance (^{1}H NMR) spectrum of SMDM was recorded using an AVANCE IIITM HD 400 MHz NanoBAY NMR spectrometer (Bruker, Germany) with D_2O as the solvent. Fourier transform infrared spectrum (FTIR) of SMDM was recorded on a spectrometer (Nicolet 6700, USA) in the range of 400 ~ 4000 cm^{-1}.

The X-ray diffraction (XRD) measurement of Ag NPs and nanocomposite coatings was carried out on a X-ray diffractometer (Rigaku Ultima IV, Japan) in a range of $2\theta = 5°\sim90°$, using Cu Kα radiation ($\lambda = 0.15406$ nm) as X-ray source, operated at 40 kV and 40 mA.

Dynamic Light Scattering (DLS) and Zeta potential measurements were performed with BI-90Plus laser particle size analyzer/Zeta potential analyzer (Brookhaven) to characterize the particle size and Zeta potential of different samples. Samples were diluted to an appropriate concentration in deionized water before measurements and then were sonicated for a period of time.

The morphologies of Ag NPs and nanocomposite emulsions were observed by JEM-2100F transmission electron microscope (TEM) manufactured by JEOL. Particularly, the size and dispersion state of Ag NPs in the polymer matrix were observed via TEM to tell whether Ag NPs were uniformly dispersed.

The morphologies of the coating cross sections were characterized by scanning electron microscope (SEM, Hitachi, S-4800, Japan) equipped with an X-MAX20 energy dispersive spectrometer (EDS) (Oxford).

The surface morphologies of the prepared coatings was detected by atomic force microscope (AFM) (CSPM5500A, Benyuan Nano-Instruments Ltd., China) and the quantitative roughness of the coatings was calculated using the Imager software in terms of average roughness (R_a) and root mean square roughness (R_q).

Water contact angles (WCA) of the prepared coatings and their evolution with time were measured at room temperature with a 5 μL deionized water drops by using a JC 2000D CA meter (Shanghai Zhongchen Instrument Co. Ltd., China). Each coating was tested in three parallels. According to Owens-Wendt-Kaelble (OWK) method [42,43], the surface energy of the coatings was measured and calculated by the JC 2000D software. Deionized water and decahydronaphthalene were used as the test liquids respectively. Both water and decahydronaphthalene contact angles were used by the initial value. Each test was conducted in triplicates.

The tensile testing of P(MMA-co-BA), P(MMA-co-BA)/SDS/$Ag_{2.50}$ and P(MMA-co-BA-co-SMDM)/Ag was performed on a universal testing machine (M350-20KN, Testometric, UK) at a 2 mm/min crosshead speed at room temperature. The limit of force transducer was 500 N (BSA-XS-50 kg). The dimensions of tensile specimens were 25 × 5 × 0.25 mm. Each coating was tested in five parallels.

2.6. Antibacterial tests

The evaluation of the antibacterial activity of the prepared coatings was thoroughly determined and discussed by the following methods: the inhibition zone method, the plate colony assay and the optical density of bacterial count method. *E. coil* and *S. aureus* were used in the antibacterial experiment as typical Gram-negative and Gram-positive bacteria, respectively. The nanocomposite coatings were made into small circular samples with a diameter of 1 cm by a puncher, which were sterilized by ultraviolet radiation for more than 2 h before the microbiological experiments.

The antibacterial capability of the prepared coatings was firstly investigated using the inhibition zone method which is also called the agar disk diffusion method. The sterilized circular samples were placed on *E. coli* and *S. aureus* bacterial agar plates with the inoculum concentration of 3×10^7 colonies forming units per mL (CFU/mL), respectively, which were then incubated in a shaking incubator at 37 °C and 80 rpm for 18 h. Three replicate experiments were performed. The presence of the inhibition zones was recorded by a digital camera and the diameters of the inhibition zones were measured. Zones of inhibition were presented as the diameter of the area of no bacterial growth minus the diameter of the sample itself. The antibacterial effect can be characterized by the presence and size of inhibition zones.

Then, the killing efficiency of the prepared coatings against bacteria was characterized by the plate colony assay. Briefly, the bacterial suspension was diluted by 1000 times to achieve a loading of 3×10^5 CFU/mL. Subsequently, 200 μL of this bacterial suspension and 600 μL of liquid culture medium were added into each well of the 24-well plate with the coating samples. The blank group contained only 200 μL bacterial suspension and 600 μL liquid culture medium. The 24-well plate was incubated at 80 rpm for 24 h at 37 °C. A certain amount of the bacterial suspension was then taken from per well and diluted with an appropriate dilution factor. The diluted bacterial suspension (10 μL) was scraped uniformly onto a nutrient agar (Biotopped®, life sciences) plate and cultured at 37 °C for 18 h. The number of colony-forming units was recorded after incubation and the bacteria count was expressed as the CFU number per sample. Each test was conducted in triplicates.

In addition, the optical density (OD) of bacterial count method was used to demonstrate the bactericidal ability of different samples more accurately and quantificationally. The optical density value at 600 nm (OD_{600}) of the remaining bacterial suspension in the plate colony assay was measured by the Microplate Reader (TECAN, Switzerland). For *E. coli* and *S. aureus*, each test was conducted in triplicates. The lower the OD_{600} value, the less the bacterial content and the better the antibacterial effect.

The long-lasting and stable antibacterial effect of the coatings was also investigated through the optical density method. In short, the bacterial suspension was diluted 1000 times to 3×10^5 CFU/mL and then the coating samples were placed in each well of the 24-well plate, followed by the addition of 200 μL of the bacterial suspension and 1000 μL of liquid culture medium to each well. The 24-well plate was incubated at 80 rpm for 7 days at 37 °C. The blank group contained only 200 μL bacterial suspension and 1000 μL liquid culture medium. Additional 200 μL of the bacterial suspension was added after every 24 h to provide new sources of bacteria. The coating samples were taken out from the 24-well plate every 24 h and the OD_{600} values of the bacterial suspension was measured via the Microplate Reader. Each test was conducted in triplicates. The growth inhibition rate was defined by the following equation:

$$\text{Growth inhibition rate}\,(\%) = (OD_{\text{Positive control}} - OD_{\text{Samples}}) / (OD_{\text{Positive control}} - OD_{\text{Negative control}}) \times 100$$

where $OD_{\text{Positive control}}$, $OD_{\text{Negative control}}$ and OD_{Samples} represent the OD_{600} values of the bacterial suspension without the coating samples,

the pure liquid culture medium, and the bacterial suspension with the coating samples, respectively.

SEM was employed to evaluate the attachment and biofilm formation of *E. coli* and *S. aureus* on different coating surfaces. In brief, the coatings were immersed in the bacterial suspension (3×10^5 CFU/mL) and a certain amount of liquid culture medium, followed by incubation at 37 °C for 7 days. An appropriate amount of liquid culture medium was added after every 24 h to prevent the bacteria culture medium from drying out. At the predetermined time points, the coatings were washed thrice with sterile phosphate buffer saline (PBS), followed by fixation with 2.5% glutaraldehyde in PBS overnight. After fixation, the coatings were washed thrice again with sterile PBS. The fixed bacteria were dehydrated with a series of graded ethanol solution (25%, 50%, 75%, 95%, and 100%, 10 min each). The coatings were sputter-coated with a gold layer and observed under SEM (Hitachi, S-4800, Japan).

3. Results and discussion

3.1. Preparation and characterization of nanocomposite emulsions and coatings

3.1.1. TEM analysis

TEM images of Ag NPs dispersed in deionized water by ultrasound and polymer nanocomposite emulsions are shown in Fig. 2. Despite a long period of ultrasonic dispersion, Ag NPs still exhibit very severe agglomeration in water with particle size more than 200 nm (Fig. 2a) and when Ag NPs/SMDM were dispersed in deionized water, the dispersion of Ag NPs is greatly improved (Fig. 2b). It can be found from the TEM image of P(MMA-co-BA)/SDS/$Ag_{2.50}$ (Fig. 2c) that the dispersion of Ag NPs in the polymer matrix is uneven and significant agglomeration occurred, indicating that SDS as a traditional emulsifier cannot successfully disperse nanoparticles and prepare polymer nanocomposite emulsions. Due to the action of SMDM, different amounts of Ag NPs achieves relatively uniform dispersion in the polymer matrix. The difference is that less addition of Ag NPs (1.25 wt%) results in lower loading and sparse distribution of Ag NPs (Fig. 2d, d'), while more addition of Ag NPs (3.75 wt%) results in relatively poor dispersion of Ag NPs (Fig. 2f, f'), and the addition of 2.50 wt% Ag NPs (Fig. 2e, e') achieves a double guarantee of the loading and dispersibility of Ag NPs, so 2.50 wt% is the optimal addition amount among the three contents. From the TEM images, it can be observed that the particle sizes of Ag NPs after successful dispersion are around 5 nm, which demonstrates that SMDM can indeed achieve uniform dispersion of Ag NPs in the polymer. In addition, the mechanical performance of coatings are closely related to the dispersion state of Ag NPs. As shown in Fig. S4 and Table S1, the mechanical performance testing results are completely consistent with the TEM results, which strongly demonstrates the role of SMDM in dispersing Ag NPs. The mechanism of SMDM as polymerizable emulsifier/anionic ligand for uniform dispersion of Ag NPs is shown in Fig. 1.

3.1.2. DLS analysis

The DLS results of particle sizes of commercial Ag NPs directly dispersed in water, Ag NPs/SMDM dispersed in water and particles in P(MMA-co-BA) and polymer nanocomposite emulsions are shown in Fig. 3, and the specific values of the intensity-average particle size and polydispersity index (PDI) are listed in Table 1. As shown in Fig. 3a, the particle size of commercial Ag NPs dispersed in aqueous medium is large and the intensity-average particle size reaches 241.7 ± 41.5 nm, indicating that the agglomeration is serious. However, when Ag NPs/SMDM were dispersed in water, the particle size of Ag NPs shows a huge drop (Fig. 3b), and the intensity-average particle size is sharply reduced to 15.8 ± 1.3 nm, demonstrating strong electrostatic interaction between Ag NPs and SMDM. In addition, the intensity-average particle sizes of pure polymer P(MMA-co-BA) (Fig. 3c) and polymer nanocomposite emulsions (Fig. 3d-g) are 107.0 ± 18.9 nm, 131.6 ± 32.6 nm, 114.1 ± 25.3 nm, 118.0 ± 26.5 nm and 135.8 ± 28.5 nm, respectively. Considering the TEM results, it indicates that Ag NPs achieve a relatively uniform dispersion in the polymer matrix. Furthermore, compared with the control experiments, the particle sizes of the polymer microspheres are all a little more than 100 nm, indicating that SMDM has a good effect as an emulsifier. In addition, as shown in Table 1, the PDI value of P(MMA-co-BA)/SDS/$Ag_{2.50}$ is 0.324 ± 0.036, while the PDI values of P(MMA-co-BA-co-SMDM)/Ag are 0.294 ± 0.022, 0.284 ± 0.013 and 0.286 ± 0.020, respectively, which are all close to pure P(MMA-co-BA) (0.287 ± 0.012) and obviously less than 0.324 ± 0.036, illustrating that SMDM maintains the uniformity of polymer particle size distribution while introducing Ag NPs into the polymer matrix.

3.1.3. Zeta potential analysis

Zeta potential values provide strong evidence of the electrostatic interaction between SMDM and Ag NPs [44] and are indicative of the homogeneity and stability of polymer nanocomposite emulsions [45]. Zeta potential measurements are presented in Table 1. As shown in Table 1, Ag NPs display a positive zeta potential around 16.27 ± 0.569 mV and SMDM shows a strong negative zeta potential around −86.35 ± 2.155 mV. However, because of the electrostatic interaction between the negative potential of SMDM and the positive potential on the surface of Ag NPs, when Ag NPs/SMDM were dispersed in water, they exhibit a zeta potential of −55.39 ± 3.145 mV. Additionally, zeta potential values of P(MMA-co-BA), P(MMA-co-BA)/SDS/$Ag_{2.50}$, P(MMA-co-BA-co-SMDM)/$Ag_{1.25}$, P(MMA-co-BA-co-SMDM)/$Ag_{2.50}$ and P(MMA-co-BA-co-SMDM)/$Ag_{3.75}$ are −96.63 ± 2.248 mV, −84.23 ± 6.051 mV, −69.34 ± 5.499 mV, −63.98 ± 1.327 mV and −56.91 ± 1.748 mV, respectively. Compared with P(MMA-co-BA) and P(MMA-co-BA)/SDS/$Ag_{2.50}$, the zeta potential of P(MMA-co-BA-co-SMDM)/Ag emulsions is significantly increased, also demonstrating the strong electrostatic interaction between SMDM and Ag NPs. In addition, the stability of the emulsions is improved as the absolute value of the zeta potential increases and when the absolute value of the zeta potential is greater than 30 mV, the emulsion stability is high [45,46]. Although the zeta potential of the P(MMA-co-BA-co-SMDM)/Ag emulsions is increased, the absolute values are far greater than 30 mV, indicating that P(MMA-co-BA-co-SMDM)/Ag emulsions still have high stability.

3.1.4. XRD analysis

Fig. 4 exhibits the XRD patterns of Ag NPs, P(MMA-co-BA), P(MMA-co-BA)/SDS/$Ag_{0.25}$ and P(MMA-co-BA-co-SMDM)/Ag. Ag NPs show the peaks at 2θ values of 38.3°, 44.4°, 64.6°, 77.5° and 81.7°, which are assigned to the (1 1 1), (2 0 0), (2 2 0), (3 1 1) and (2 2 2) diffractions of Ag, respectively, suggesting the commercial Ag NPs are face-centered cubic (fcc) with high crystallinity [28]. And the pure P(MMA-co-BA) is amorphous and has a broad band centered at 2θ ≈ 19°, which is ascribed to the periodicity in parallel chains. Surprisingly, P(MMA-co-BA)/SDS/$Ag_{2.50}$ exhibits almost the same XRD pattern as pure P(MMA-co-BA) and no diffraction peaks of Ag NPs are observed, which means that very small amounts of Ag NPs were introduced into the polymer matrix, suggesting that SDS cannot successfully combine Ag NPs with polymer matrix. On the other hand, similar five sharp diffraction peaks of Ag NPs and a broad diffraction band of pure polymer are observed in the P(MMA-co-BA-co-SMDM)/Ag. From this result, it is inferred that Ag NPs were incorporated into the polymer matrix through the effect of SMDM. So compared with SDS, SMDM improves the bonding, compatibility and interaction between Ag NPs and polymer matrix. Moreover, the preparation of P(MMA-co-BA-co-SMDM)/Ag by emulsion copolymerization did not change the crystalline structure of Ag NPs.

3.1.5. SEM and EDS analysis

In order to investigate the dispersion state of Ag NPs in the formed coatings, P(MMA-co-BA), P(MMA-co-BA)/SDS/$Ag_{2.50}$, and P(MMA-co-

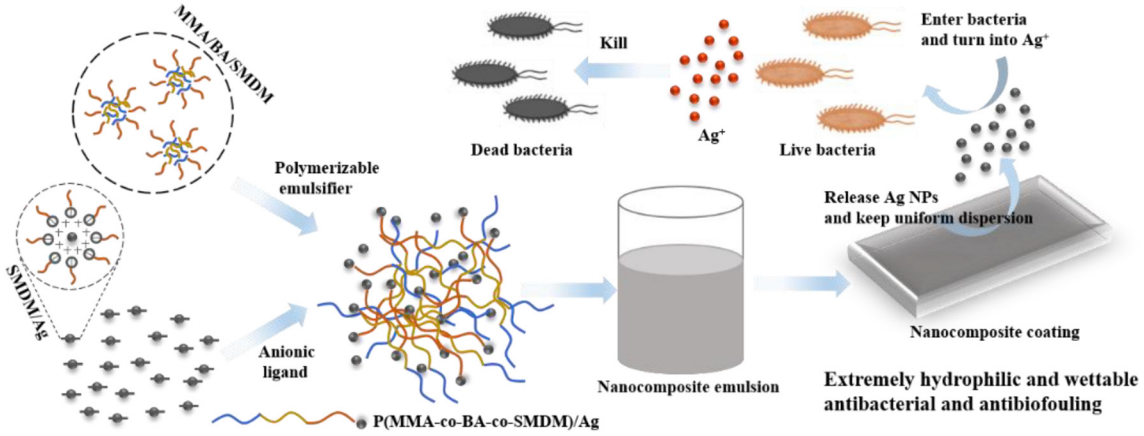

Fig. 1. Schematic diagram of SMDM as polymerizable emulsifier/anionic ligand for uniform dispersion of Ag NPs, and preparation of nanocomposite antibacterial coating and antibacterial mechanism.

BA-co-SMDM)/$Ag_{2.50}$ were selected to study their cross-sectional morphologies by SEM, and the elemental distribution was studied by EDS. As shown in Fig. 5, the cross sections of P(MMA-co-BA) (Fig. 5a) and P(MMA-co-BA)/SDS/$Ag_{2.50}$ (Fig. 5b) both exhibits a "ridge-valley" structure. Interestingly, the cross-sectional morphology of P(MMA-co-BA-co-SMDM)/$Ag_{2.50}$ (Fig. 5c) becomes smoother, which is attributed to the valley area filling with Ag NPs. This indicates that Ag NPs were introduced and uniformly dispersed in the polymer matrix. Moreover, the EDS study confirms the existence of C, O, Na and Ag elements in P (MMA-co-BA-co-SMDM)/$Ag_{2.50}$ (Fig. 5c') and reveals that Ag elements are homogeneously distributed throughout the coating, while there are only C, O, Na and S elements in the EDS mapping of P(MMA-co-BA)/SDS/$Ag_{2.50}$ (Fig. 5b'). SEM and EDS analysis of the cross sections demonstrate that Ag NPs remain uniformly dispersed in the formed P (MMA-co-BA-co-SMDM)/$Ag_{2.50}$ coating.

3.2. Surface properties of the coatings

3.2.1. AFM analysis

The surface morphology, roughness and uniformity of the different coatings were investigated by AFM. As shown in Fig. 6, the P(MMA-co-BA) exhibits a "small hills" structure and has R_a (average roughness) of 11.6 ± 0.51 nm and R_q (root mean square roughness) of 13.9 ± 0.56 nm, while the surface roughness of P(MMA-co-BA)/SDS/$Ag_{2.50}$ is reduced with R_a of 7.4 ± 0.76 nm and R_q of 10.5 ± 0.85 nm. Compared with P(MMA-co-BA), the surface roughness of P(MMA-co-BA-co-SMDM)/Ag is increased with R_a of 12.8 ± 0.66 nm, 13.0 ± 0.59 nm, 13.3 ± 0.69 nm and R_q of 15.5 ± 0.71 nm, 15.5 ± 0.65 nm, 15.8 ± 0.73 nm, respectively. In addition, the uneven surface structure leads to a larger surface area for bacteria and foulants to contact, and provides space for them to accumulate. Although the roughness is increased, due to the introduction and uniform dispersion of Ag NPs which are filled into the gaps between the "small hills" structures, the "small hills" structures in the surface of P(MMA-co-BA-co-SMDM)/Ag are significantly reduced and the surface uniformity is greatly improved. However, the surface uniformity of P(MMA-co-BA) and P(MMA-co-BA)/SDS/$Ag_{2.50}$ is poor, which provides the possibility of adhesion of bacteria and foulants [47].

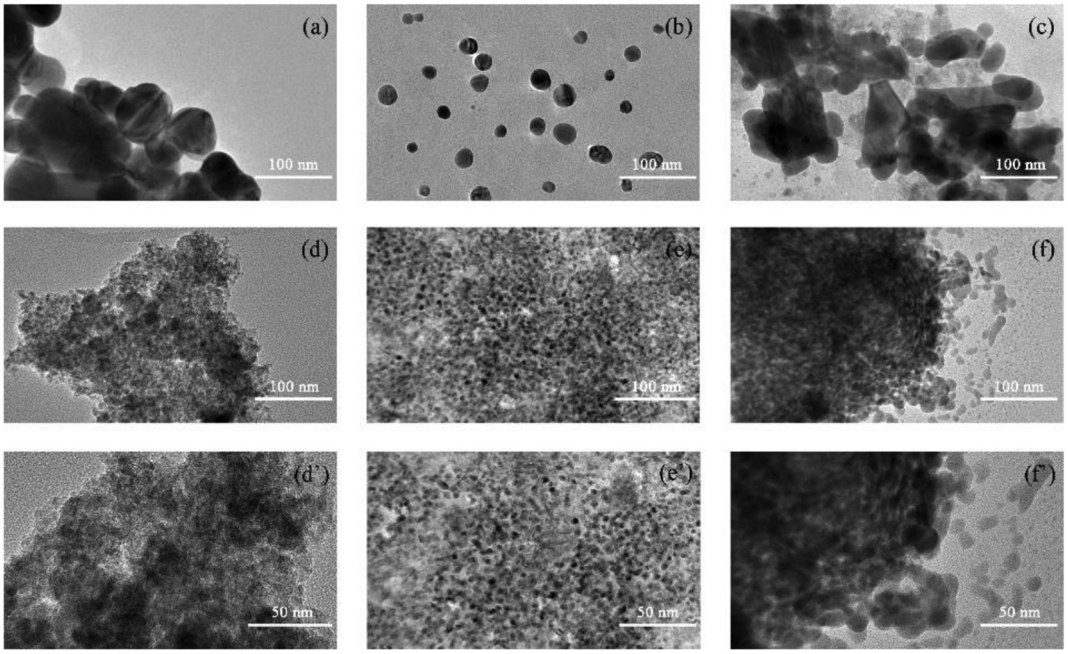

Fig. 2. TEM images of (a) Ag NPs directly dispersed in deionized water, (b) Ag NPs/SMDM dispersed in deionized water, (c) P(MMA-co-BA)/SDS/$Ag_{2.50}$, (d, d') P (MMA-co-BA-co-SMDM)/$Ag_{1.25}$, (e, e') P(MMA-co-BA-co-SMDM)/$Ag_{2.50}$ and (f, f') P(MMA-co-BA-co-SMDM)/$Ag_{3.75}$.

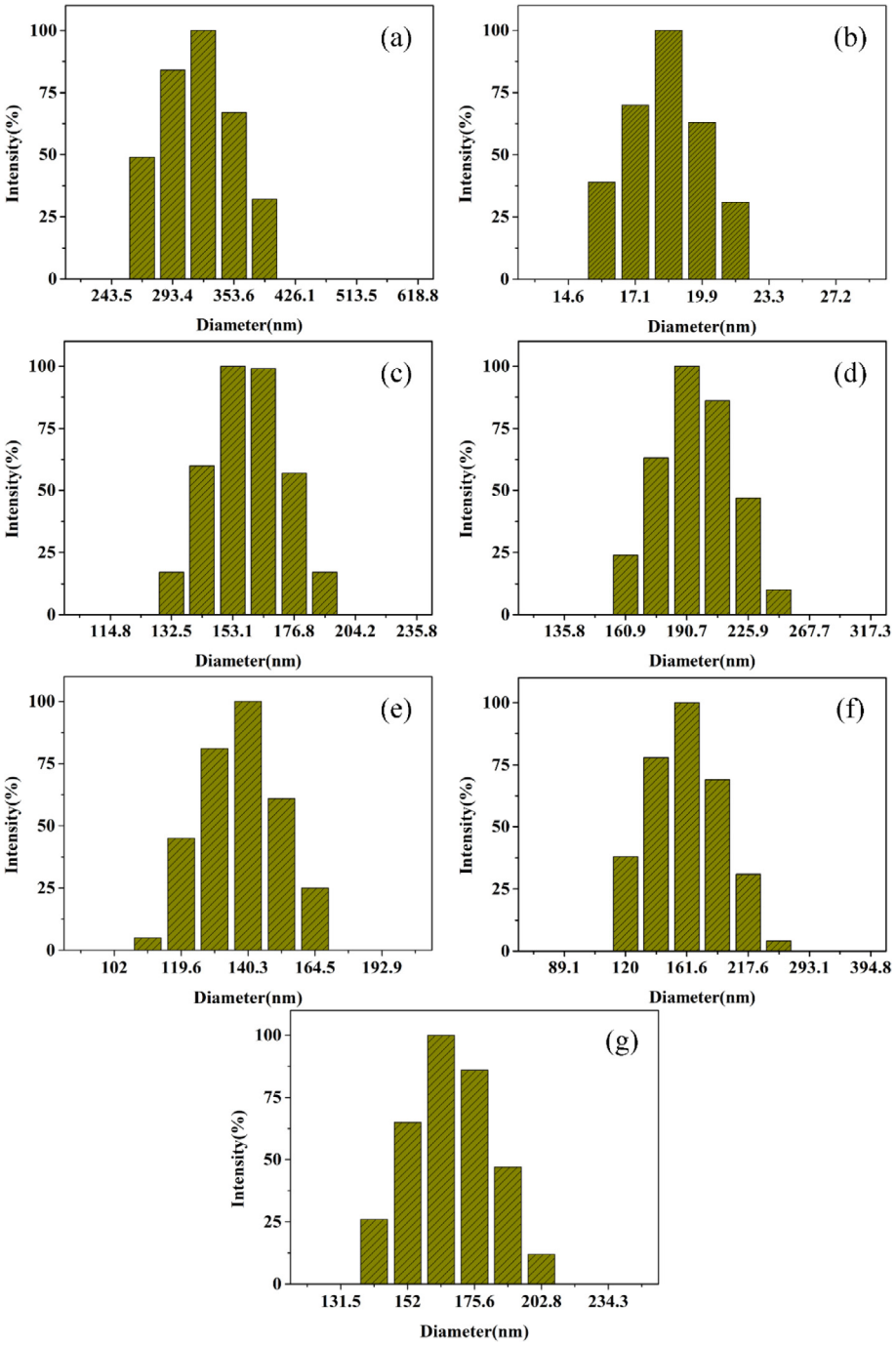

Fig. 3. Particle size distribution of (a) Ag NPs directly dispersed in deionized water, (b) Ag NPs/SMDM dispersed in deionized water, (c) P(MMA-co-BA), (d) P(MMA-co-BA)/SDS/$Ag_{2.50}$, (e) P(MMA-co-BA-co-SMDM)/$Ag_{1.25}$, (f) P(MMA-co-BA-co-SMDM)/$Ag_{2.50}$ and (g) P(MMA-co-BA-co-SMDM)/$Ag_{3.75}$ determined by DLS.

Table 1
Intensity-average particle size, polydispersity index and zeta potential of the samples.

Samples	Intensity-average particle size (nm)	Polydispersity index (PDI)	Zeta potential (mV)
Ag NPs	241.7 ± 41.5	0.222 ± 0.032	16.27 ± 0.569
SMDM	–	–	−86.35 ± 2.155
Ag NPs/SMDM	15.8 ± 1.3	0.259 ± 0.014	−55.39 ± 3.145
P(MMA-co-BA)	107.0 ± 18.9	0.287 ± 0.012	−96.63 ± 2.248
P(MMA-co-BA)/SDS/$Ag_{2.50}$	131.6 ± 32.6	0.324 ± 0.036	−84.23 ± 6.051
P(MMA-co-BA-co-SMDM)/$Ag_{1.25}$	114.1 ± 25.3	0.294 ± 0.022	−69.34 ± 5.499
P(MMA-co-BA-co-SMDM)/$Ag_{2.50}$	118.0 ± 26.5	0.284 ± 0.013	−63.98 ± 1.327
P(MMA-co-BA-co-SMDM)/$Ag_{3.75}$	135.8 ± 28.5	0.286 ± 0.020	−56.91 ± 1.748

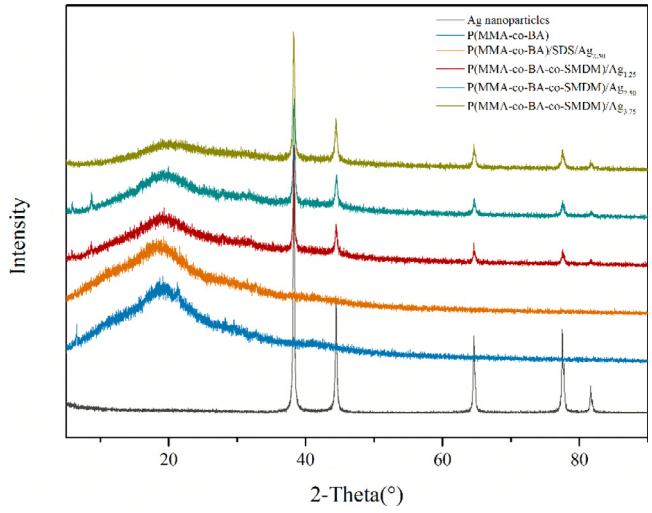

Fig. 4. XRD patterns of Ag NPs and the prepared coatings.

3.2.2. Hydrophilicity and wettability

The WCA measurement was used to characterize the change of hydrophilicity and wettability of the coatings. Fig. 7a shows photographs of the contact angles of different coatings at 0 s and at 330 s, respectively and Fig. 7b displays the contact angles versus time plots of various coatings. As shown in Fig. 7a, the initial water contact angles of pure P(MMA-co-BA) and P(MMA-co-BA)/SDS/$Ag_{2.50}$ are 83.6° and 82.5°, close to 90° and at 330 s, the water contact angles are 72.5° and 74.6°, respectively. At the same time, Fig. 7b shows that the water contact angles of P(MMA-co-BA) and P(MMA-co-BA)/SDS/$Ag_{2.50}$ does not change much over time. Considering the decrease in contact angles caused by the evaporation of water droplets themselves, the absorption of water by the coatings themselves can be considered to be negligible, which means both of pure P(MMA-co-BA) and P(MMA-co-BA)/SDS/$Ag_{2.50}$ have poor hydrophilicity and wettability. On the other hand, the initial water contact angles of P(MMA-co-BA-co-SMDM)/$Ag_{1.25}$, P(MMA-co-BA-co-SMDM)/$Ag_{2.50}$ and P(MMA-co-BA-co-SMDM)/$Ag_{3.75}$ are 65.0°, 37.8° and 24.7°, respectively, showing improved hydrophilicity, especially P(MMA-co-BA-co-SMDM)/$Ag_{2.50}$ and P(MMA-co-BA-co-SMDM)/$Ag_{3.75}$. In addition, the water contact angles drop significantly over time, and decrease to 13.2°, 9.5° and 0° (completely wetted) at 330 s, indicating that P(MMA-co-BA-co-SMDM)/Ag coatings have good wetting effect on water.

On the one hand, the change in the water contact angle of the coatings and the resulting change in hydrophilicity and wettability are directly related to the surface morphology and roughness of the coatings. Theory has shown that for surfaces with water contact angle of less than 90° (relatively hydrophilic), the increase in surface roughness will increase the hydrophilicity of the surface [48,49]. Due to the successful introduction of Ag NPs and uniform dispersion in the polymer matrix, more micro-nano structures or nano structures are constructed in the surfaces of P(MMA-co-BA-co-SMDM)/Ag coatings, resulting in increased surface roughness. When the surfaces of the coatings with increased surface roughness are in contact with the water droplets, in order to balance the entire system, the water droplets first spread on the solid surfaces and penetrate into the micro-nano structures or nano structures, and then the remaining water is completely spread on the surfaces of the water films.

On the other hand, hydrophilicity is closely related to surface energy: the larger the surface energy of solid is, the smaller the water contact angle will be, which means the hydrophilicity of the solid surface is stronger [50,51]. As shown in Fig. 7c, the surface energies of P(MMA-co-BA), P(MMA-co-BA)/SDS/$Ag_{2.50}$, P(MMA-co-BA-co-SMDM)/$Ag_{1.25}$, P(MMA-co-BA-co-SMDM)/$Ag_{2.50}$ and P(MMA-co-BA-co-SMDM)/$Ag_{3.75}$ are 29.01 ± 2.07, 28.27 ± 0.25, 40.28 ± 0.85, 59.50 ± 0.46 and 66.66 ± 0.33 mJ/m^2, respectively, which corresponds well with the results of the water contact angle test. The increase in surface energy of the coatings is another key factor in the improvement in hydrophilicity and wettability.

The improved hydrophilicity and wettability provides the foundation and possibility of antifouling self-cleaning properties of the coatings and makes the coatings less susceptible to be contaminated by bacteria and other contaminants [52–54].

3.3. Antibacterial and antibiofouling properties of the coatings

E. coli and *S. aureus* are the most prevalent species of Gram-negative and Gram-positive bacteria, respectively, which have become the widely used model bacteria for the antibacterial study.

The antibacterial capability of different coatings was firstly tested by the inhibition zone method and the results are presented in Fig. 8. For the inhibition zone method, antibacterial efficiency is rated “good” (zone of inhibition > 1 mm), “fairly good” (zone of inhibition ≤1 mm),

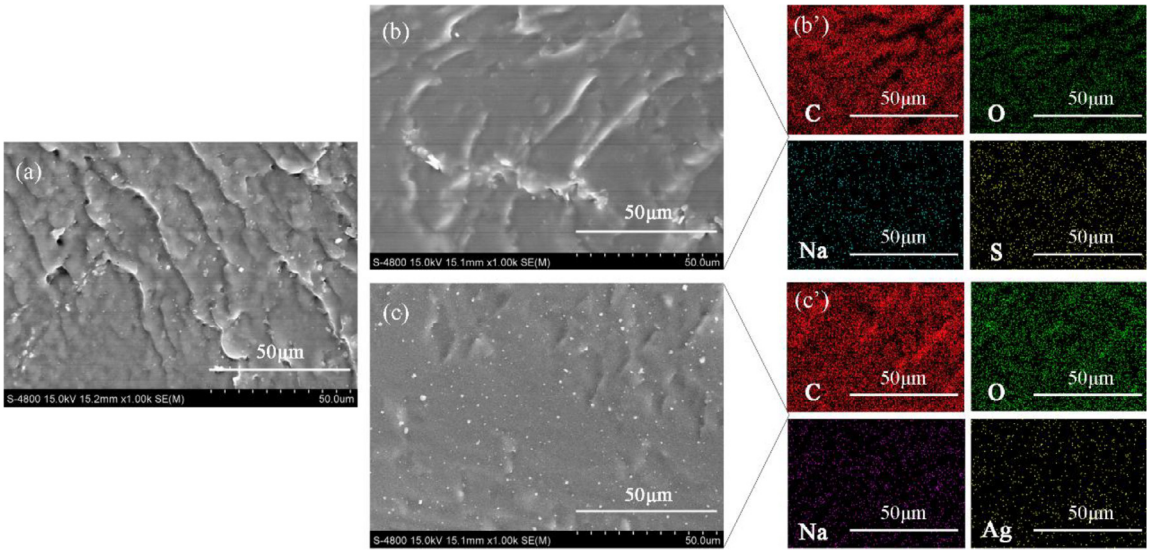

Fig. 5. Cross-sectional SEM images of (a) P(MMA-co-BA), (b) P(MMA-co-BA)/SDS /$Ag_{0.25}$, (c) P(MMA-co-BA-co-SMDM)/$Ag_{2.50}$ and cross-sectional EDS mappings of (b') P(MMA-co-BA)/SDS/$Ag_{2.50}$, (c') P(MMA-co-BA-co-SMDM)/$Ag_{2.50}$.

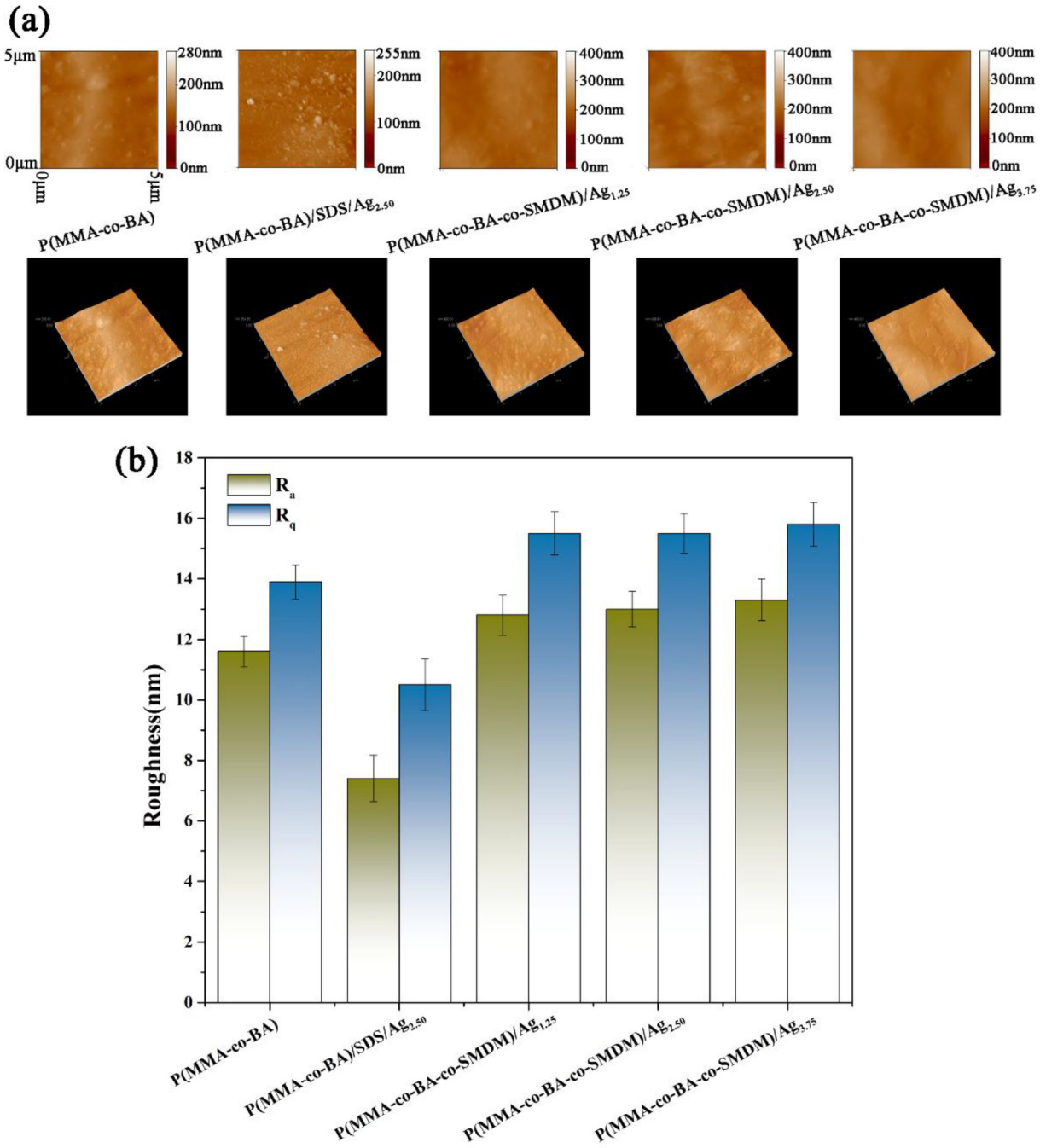

Fig. 6. AFM images (a) and roughness statistics (b) of the coating surfaces.

"sufficient" (just not growth up on the sample), "limited" (amount of growth on the sample < 50%) or "poor" (amount of growth on the sample ≥50%) [55,56].As shown in Fig. 8, P(MMA-co-BA) and P (MMA-co-BA)/SDS/$Ag_{2.50}$ have no inhibition effect on the growth of both *E. coli* and *S. aureus*, indicating that they lack antibacterial properties, while three P(MMA-co-BA-co-SMDM)/Ag coatings show excellent inhibition effect against *E. coli* and *S. aureus*, and the diameters of their inhibition zones are 2.8 ± 0.27 mm, 2.8 ± 0.20 mm, 2.0 ± 0.25 mm and 3.1 ± 0.20 mm, 3.0 ± 0.10 mm, 2.4 ± 0.15 mm, respectively. Interestingly, P(MMA-co-BA-co-SMDM)/$Ag_{1.25}$ and P(MMA-co-BA-co-SMDM)/$Ag_{2.50}$ have relatively close inhibition effect, and although P(MMA-co-BA-co-SMDM)/$Ag_{3.75}$ has a higher amount of Ag NPs added, it has worse inhibition effect, which is related to the relatively poor dispersion of Ag NPs.

In order to further and quantitatively investigate the improvement of P(MMA-co-BA-co-SMDM)/Ag for antibacterial properties, the plate colony assay [53] and the optical density of bacterial count method [52] were adopted. As shown in Fig. 9a and b, after incubation, the blank group and P (MMA-co-BA) both formed many colonies and Log_{10}(CFU/mL) values are 5.996 ± 0.646, 6.893 ± 0.458 and 5.851 ± 0.547, 6.583 ± 0.181, respectively (Table 2), indicating poor killing efficiency for bacteria. In contrast, three P(MMA-co-BA-co-SMDM)/Ag coatings exhibit outstanding antibacterial properties without any colony growth, suggesting close to 100% killing efficiency. So as to determine the antibacterial ability and killing efficiency of P (MMA-co-BA-co-SMDM)/Ag more comprehensively, the OD_{600} values of the cultured bacterial suspension were tested, and the results are shown in Fig. 9c. Compared with blank group and P(MMA-co-BA), the OD_{600} values of P(MMA-co-BA-co-SMDM)/Ag all significantly fall, which means that the bacterial amounts were significantly reduced for

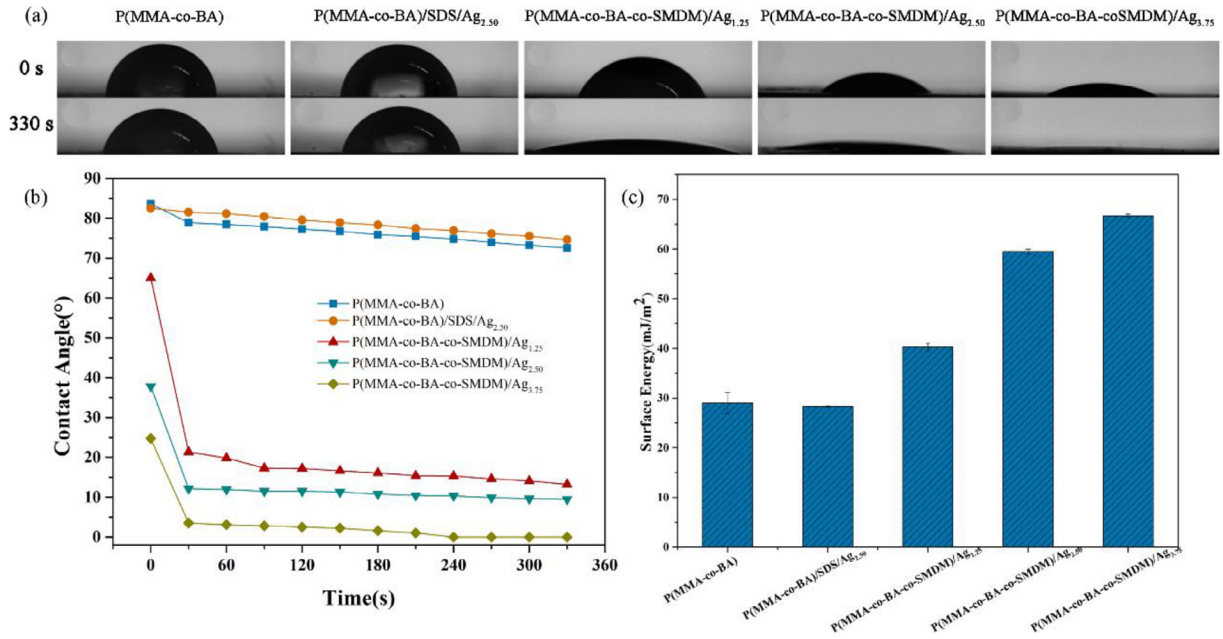

Fig. 7. WCA at 0 s and at 330 s (a), evolution of water contact angles on the coating surfaces with the time in 330 s (b) and surface energy (c).

both *E. coli* and *S. aureus*. In addition, P(MMA-co-BA-co-SMDM)/$Ag_{2.50}$ shows the smallest OD_{600} values for both *E. coli* and *S. aureus*.

The long-lasting and stable antibacterial effect is critical for antibacterial coatings [57,58]. The durability of the coatings' antibacterial properties was monitored by testing the OD_{600} values in 7 days and the growth inhibition rate was calculated. As shown in Fig. 10, for *E. coli* (Fig. 10a) and *S. aureus* (Fig. 10b), the OD_{600} values of the blank group and P(MMA-co-BA) are both much larger and increase over time. Surprisingly, the OD_{600} value of P(MMA-co-BA) even exceeds the blank group over time. This may be due to the fact that during the long-term culture, some substances of the P(MMA-co-BA) coating were dissolved in the liquid culture medium, which lead to an increase in absorbance, and the coating also provided more attachment sites for the bacteria, promoting the growth of the bacteria. In sharp contrast, three P(MMA-co-BA-co-SMDM)/Ag coatings demonstrate the outstanding bacteriostatic effect against *E. coli* and *S. aureus* and do not change basically over time. Furthermore, their growth inhibition rates against *E. coli* (Fig. 10c) and *S. aureus* (Fig. 10d) keep basically constant and even on the seventh day, the growth inhibition rates against *E. coli* and *S. aureus* still remain at 91.5 ± 2.40%, 96.5 ± 3.11%, 98.9 ± 1.11% and 89.8 ± 2.53%, 96.1 ± 3.67%, 99.8 ± 0.18%, respectively. In fact, excluding the experimental error caused by the long-term culture process, it is basically considered that P(MMA-co-BA-co-SMDM)/$Ag_{2.50}$ and P(MMA-co-BA-co-SMDM)/$Ag_{3.75}$ always maintained a growth inhibition rate of nearly 100% for 7 days. The durability and stability of antibacterial properties lay a solid foundation for the practical application of P(MMA-co-BA-co-SMDM)/Ag coatings.

Biofilm on coating surfaces consists of bacteria, their secreted extracellular matrix, and organic debris is extremely difficult to remove and once the biofilm is formed, it can have a fatal effect on the

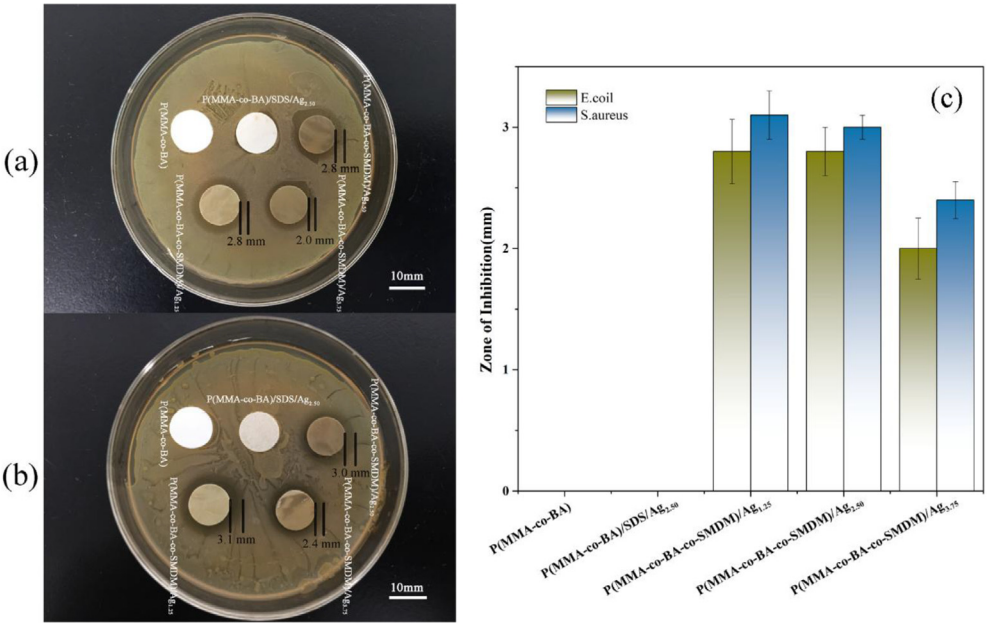

Fig. 8. Photographs of bacterial inhibition zones of different coatings towards *E. coli* (a) and *S. aureus* (b), and diameters of inhibition zones (c) of different coatings.

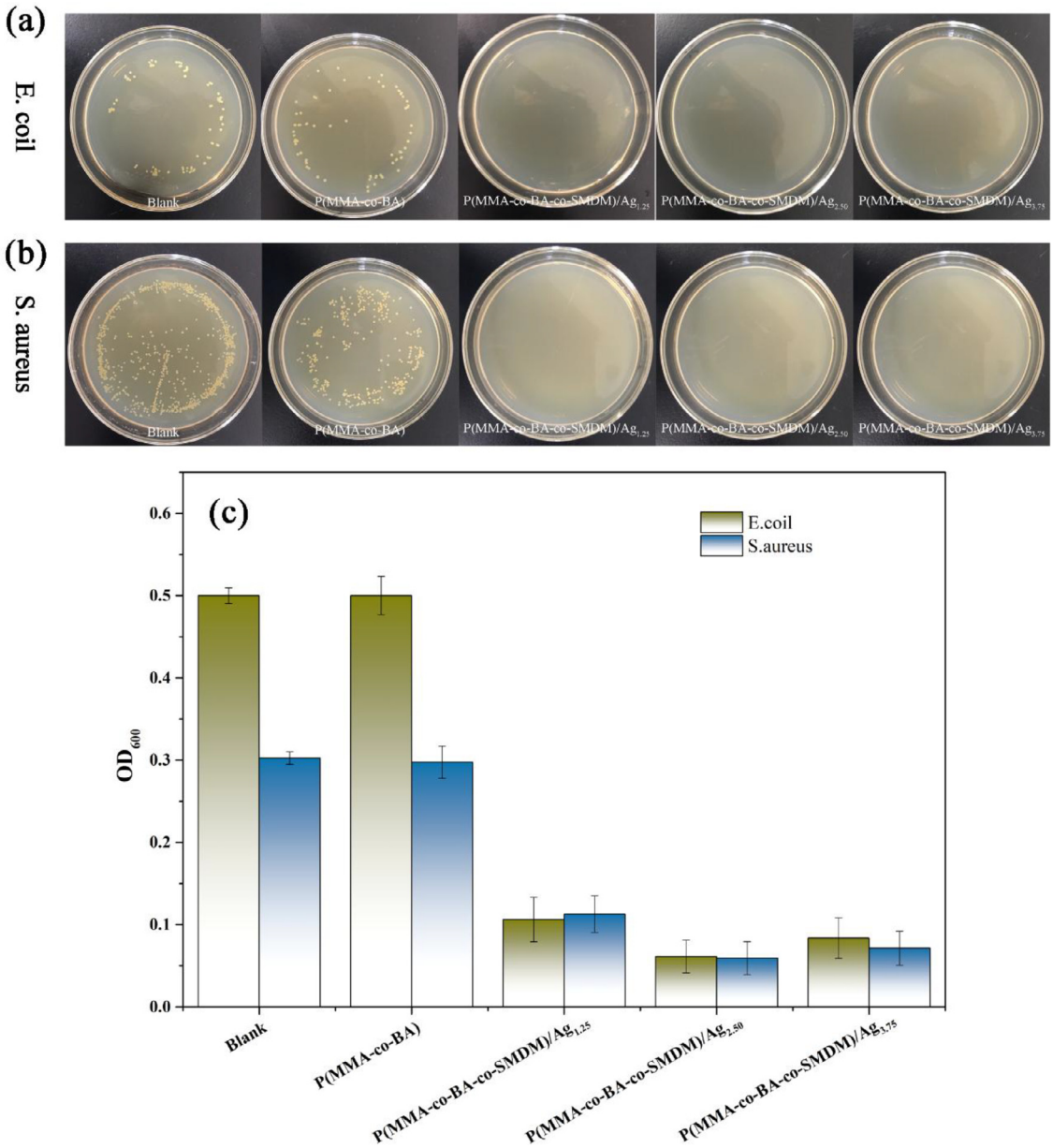

Fig. 9. Digital images of viable colonies of *E. coli* (a) and *S. aureus* (b) via plate colony assay, and OD_{600} values (c) of different bacterial suspensions.

performance of the coatings [53]. As shown in Fig. 11 and Fig. S6, a large amount of bacteria adhered to the surface of P(MMA-co-BA) coating which developed both *E. coli* and *S. aureus* biofilms at 7 days and the thick biofilms almost covered the whole surfaces. Bacterial clusters and agglomerates of substances produced by bacteria can be clearly observed on the coating surfaces, indicating that P(MMA-co-BA) coating is unable to prevent bacterial adhesion and biofilm formation. In sharp contrast, three P(MMA-co-BA-co-SMDM)/Ag coatings almost completely inhibited bacteria fouling and adhesion, effectively preventing biofilm formation of both *E. coli* and *S. aureus*. Studies have demonstrated that increased surface hydrophilicity reduces bacterial adhesion and prevents biofilm formation [52,53]. As described above, due to the large increase in hydrophilicity, the biofilm formation on the coating surfaces is greatly suppressed. Effective inhibition of biofilm formation has great significance for maintaining the properties and further applications of the coating.

The antibacterial effect of Ag NPs is greatly influenced by the particle size: the smaller the Ag NPs, the greater antibacterial activity.

Table 2
Viable colony counts of *E. coli* and *S. aureus*.

Samples	Log_{10}(CFU/mL) (*E. coil*)	Log_{10}(CFU/mL) (*S. aureus*)
Blank	5.996 ± 0.646	6.893 ± 0.458
P(MMA-co-BA)	5.851 ± 0.547	6.583 ± 0.181
P(MMA-co-BA-co-SMDM)/$Ag_{1.25}$	–	–
P(MMA-co-BA-co-SMDM)/$Ag_{2.50}$	–	–
P(MMA-co-BA-co-SMDM)/$Ag_{3.75}$	–	–

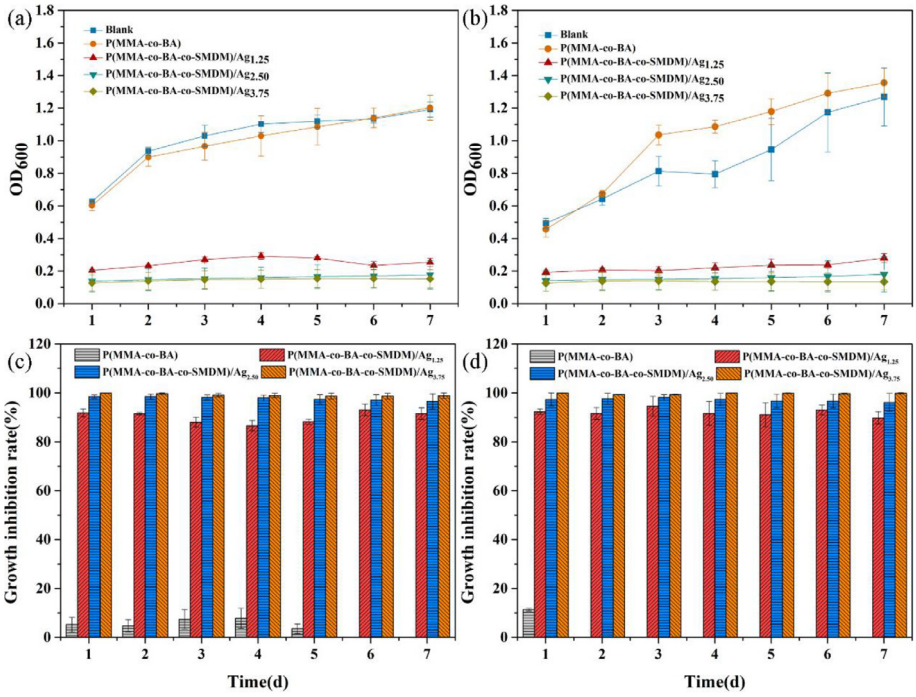

Fig. 10. Evolution of OD_{600} values of bacterial suspensions towards *E. coil* (a) and *S. aureus* (b), and growth inhibition rate of different coatings against *E. coil* (c) and *S. aureus* (d) during 7 days.

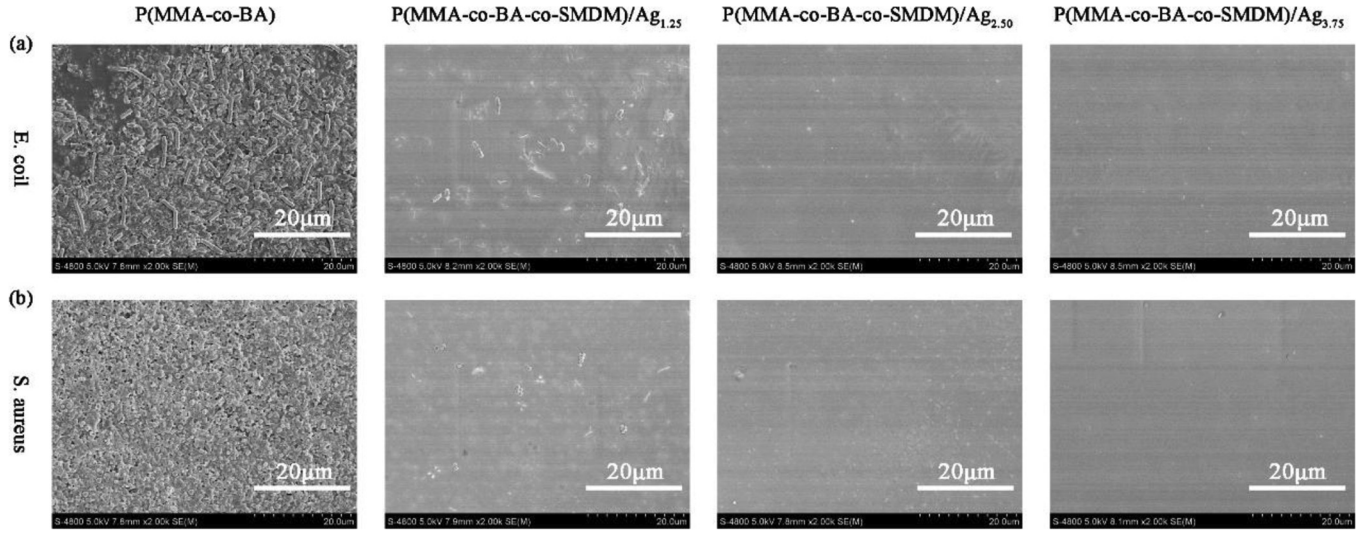

Fig. 11. SEM images of *E. coli* (a) and *S. aureus* (b) after 7 days of incubation on coating surfaces.

Studies found that Ag NPs with a particle size of about 20 nm are difficult to enter the bacteria and only when the particle size is less than 10 nm, especially around 5 nm, can they enter the interior of the bacteria [26]. As a result, the antibacterial effect of Ag NPs with a particle size of about 5 nm is significantly better. The TEM results (Fig. 2) illustrate that the aggregation of Ag NPs in P(MMA-co-BA)/SDS/$Ag_{2.50}$ is serious, completely inhibiting the antibacterial action of Ag NPs. In P(MMA-co-BA-co-SMDM)/$Ag_{1.25}$ and P(MMA-co-BA-co-SMDM)/$Ag_{2.50}$, Ag NPs are uniformly dispersed in the polymer matrix with a particle size of about 5 nm and the difference is that the content of Ag NPs in P(MMA-co-BA-co-SMDM)/$Ag_{1.25}$ is less, so the antibacterial effect is relatively poor. When the amount of Ag NPs increases to a higher value (3.75 wt%), the dispersibility of Ag NPs is relatively reduced and the particle size increases to more than 10 nm, thus leading to a negative impact on antibacterial properties. So compared with P(MMA-co-BA-co-SMDM)/$Ag_{2.50}$, P(MMA-co-BA-co-SMDM)/$Ag_{3.75}$ presents similar or even weaker antibacterial effect, which also proves that uniform dispersion of Ag NPs rather than content has the most crucial influence on the antibacterial properties.

Since the well-known bioactivity, Ag NPs have been widely used to prevent bacterial contamination. The antibacterial mechanism of Ag NPs is attributed to surface oxidation and subsequent release of Ag ions, which can interact with DNA or the thiol groups in proteins, to result in the interruption of DNA replication, or the inactivation of respiratory enzymes of bacterial [23]. Considering the antibacterial mechanism of Ag NPs, it is crucial that Ag NPs are released from polymer coating and contact with bacteria (Fig. 1). As discussed previously, the hydrophilicity and wettability of P(MMA-co-BA-co-SMDM)/Ag coatings are significantly improved. Therefore, the coatings slightly swell by absorbing moisture or water vapor in the air, causing an increase in the

distance between the polymer segments, and Ag NPs are more easily released from the coatings and contact with bacteria, thus producing good antibacterial effect.

4. Conclusions

In summary, we reported a simple, efficient and environmentally friendly method for preparing a polymer nanocomposite coating with greatly improved hydrophilicity and wettability, significantly enhanced antibacterial and antibiofouling properties via emulsion polymerization. In this work, SMDM was successfully synthesized and used as polymerizable emulsifier as well as anionic ligand to uniformly disperse Ag NPs by electrostatic interaction. Through the role of SMDM, Ag NPs achieved extremely uniform dispersion, and the particle size was reduced to about 5 nm. The coating exhibited outstanding and long-lasting antibacterial and antibiofouling properties, maintaining nearly 100% growth inhibition rate and completely preventing bacterial adhesion and biofilm formation against both *E. coil* and *S. aureus* over 7 days. Moreover, the P(MMA-co-BA-co-SMDM)/$Ag_{2.50}$ coating exhibited the best overall performance and 2.5 wt% was the relatively reasonable addition amount of Ag NPs. The prepared nanocomposite coating might have potential applications in various industrial fields. Other than this, this work provides a promising and universal idea for constructing a system in which nanoparticles are uniformly dispersed and preparing a series of functionalized polymer nanocomposite coatings.

Declaration of Competing Interest

There are no conflicts to declare.

Acknowledgments

This work is supported by National Natural Science Foundation of China (Grant No. 51473114).

Appendix A. Supplementary data

Supplementary data to this article can be found online at https://doi.org/10.1016/j.cej.2019.122268.

References

[1] W.J. Yang, K.G. Neoh, E.T. Kang, S.L.M. Teo, D. Rittschof, Polymer brush coatings for combating marine biofouling, Prog. Polym. Sci. 39 (2014) 1017–1042.
[2] S.W. Lee, H. Gu, J.B. Kilberg, D.C. Ren, Sensitizing bacterial cells to antibiotics by shape recovery triggered biofilm dispersion, Acta Biomater. 81 (2018) 93–102.
[3] X.M. Dai, Q.Q. Guo, Y. Zhao, P. Zhang, T.Q. Zhang, X.G. Zhang, C.X. Li, Functional silver nanoparticle as a benign antimicrobial agent that eradicates antibiotic-resistant bacteria and promotes wound healing, ACS Appl. Mater. Interfaces 8 (2016) 25798–25807.
[4] H.H. Wang, Y. He, G.Q. Fei, C.Y. Wang, Y.D. Shen, K. Zhu, L.Y. Sun, N.N. Rang, D.H. Guo, G.G. Wallace, Functionalizing graphene with titanate coupling agents as reinforcement for one-component waterborne poly(urethane-acrylate) anticorrosion coatings, Chem. Eng. J. 359 (2019) 331–343.
[5] J.H. Ryu, P.B. Messersmith, H. Lee, Polydopamine surface chemistry: a decade of discovery, ACS Appl. Mater. Interfaces 10 (2019) 7523–7540.
[6] Y. Yang, T. Zhang, J.J. Yan, L.W. Fu, H.P. Xiang, Y.Y. Cui, J.H. Su, X.X. Liu, Preparation and photochromic behavior of spiropyran-containing fluorinated polyacrylate hydrophobic coatings, Langmuir 34 (2018) 15812–15819.
[7] X.K. Ding, S. Duan, X.J. Ding, R.H. Liu, F.J. Xu, Versatile antibacterial materials: an emerging arsenal for combatting bacterial pathogens, Adv. Funct. Mater. 28 (2018) 1802140.
[8] M.L.W. Knetsch, L.H. Koole, New strategies in the development of antimicrobial coatings: the example of increasing usage of silver and silver nanoparticles, Polymers 3 (2011) 340–366.
[9] S.Q. Li, S.J. Dong, W.G. Xu, S.C. Tu, L.S. Yan, C.W. Zhao, J.X. Ding, X.S. Chen, Antibacterial hydrogels, Adv. Sci. 5 (2018) 1700527.
[10] F. Wahid, C. Zhong, H.S. Wang, X.H. Hu, L.Q. Chu, Recent advances in antimicrobial hydrogels containing metal ions and metals/metal oxide nanoparticles, Polymers 9 (2017) 636.
[11] A. Zajac, R. Kukawka, A. Pawlowska-Zygarowicz, O. Stolarska, M. Smiglak, Ionic liquids as bioactive chemical tools for use in agriculture and the preservation of agricultural products, Green Chem. 20 (2018) 4764–4789.
[12] M.A. Rahman, M. Bam, E. Luat, M.S. Jui, M.S. Ganewatta, T. Shokfai, M. Nagarkatti, A.W. Decho, C.B. Tang, Macromolecular-clustered facial amphiphilic antimicrobials, Nat. Commun. 9 (2018) 5231.
[13] J. Lin, X.Y. Chen, C.Y. Chen, J.T. Hu, C.L. Zhou, X.F. Cai, W. Wang, C. Zheng, P.P. Zhang, J. Cheng, Z.H. Guo, H. Liu, Durably antibacterial and bacterially anti-adhesive cotton fabrics coated by cationic fluorinated polymers, ACS Appl. Mater. Interfaces 10 (2018) 6124–6136.
[14] M. He, H.Y. Jiang, R. Wang, Y. Xie, W.F. Zhao, C.S. Zhao, A versatile approach towards multi-functional surfaces via covalently attaching hydrogel thin layers, J. Colloid Interface Sci. 484 (2016) 60–69.
[15] I. Parisi, L. Scrivano, M.S. Sinicropi, F. Puoci, Polymeric nanoparticle constructs as devices for antibacterial therapy, Curr. Opin. Pharmacol. 36 (2017) 72–77.
[16] M. Daglia, Polyphenols as antimicrobial agents, Curr. Opin. Biotech. 23 (2012) 174–181.
[17] S. Dimassi, N. Tabary, F. Chai, N. Blanchemain, B. Martel, Sulfonated and sulfated chitosan derivatives for biomedical applications: a review, Carbohyd. Polym. 202 (2018) 382–396.
[18] J.L. Liu, Z. Li, Q.R. Lin, X.J. Jiang, J.R. Yao, Y.H. Yang, Z.Z. Shao, X. Chen, A robust, resilient, and multi-functional soy protein-based hydrogel, ACS Sustain. Chem. Eng. 6 (2018) 13730–13738.
[19] M.J. Hajipour, K.M. Fromm, A.A. Ashkarran, D.J. de Aberasturi, I.R. de Larramendi, T. Rojo, V. Serpooshan, W.J. Parak, M. Mahmoudi, Antibacterial properties of nanoparticles, Trends Biotechnol. 30 (2012) 499–511.
[20] K.Y. Zheng, M.I. Setyawati, D.T. Leong, J.P. Xie, Antimicrobial silver nanomaterials, Coordin. Chem. Rev. 357 (2018) 1–17.
[21] B. Le Ouay, F. Stellacci, Antibacterial activity of silver nanoparticles: a surface science insight, Nano Today 10 (2015) 339–354.
[22] P. Dibrov, J. Dzioba, K.K. Gosink, C.C. Hase, Chemiosmotic mechanism of antimicrobial activity of Ag^+ in *Vibrio cholerae*, Antimicrob. Agents Ch. 46 (2002) 2668–2670.
[23] S. Chernousova, M. Epple, Silver as antibacterial agent: ion, nanoparticle, and metal, Angew. Chem. Int. Edit. 52 (2013) 1636–1653.
[24] K.K. Choi, N.J. Deng, L. Kim, R.Y. Ross, Z.Q. Surampalli, Hu, The inhibitory effects of silver nanoparticles, silver ions, and silver chloride colloids on microbial growth, Water Res. 42 (2008) 3066–3074.
[25] T.J. Dai, C.P. Wang, Y.Q. Wang, W. Xu, J.J. Hu, Y.Y. Cheng, A nanocomposite hydrogel with potent and broad-spectrum antibacterial activity, ACS Appl. Mater. Interfaces 10 (2018) 15163–15173.
[26] J.R. Morones, J.L. Elechiguerra, A. Camacho, K. Holt, J.B. Kouri, J.T. Ramirez, M.J. Yacaman, The bactericidal effect of silver nanoparticles, Nanotechnology 16 (2005) 2346–2353.
[27] A. Panáček, L. Kvítek, R. Prucek, M. Kolář, R. Večeřová, N. Pizúrová, V.K. Sharma, T. Nevěčná, R. Zbořil, Silver colloid nanoparticles: synthesis, characterization, and their antibacterial activity, J. Phys. Chem. B 110 (2006) 16248–16253.
[28] P. Boomi, J.A. Raj, S.P. Palaniappan, G. Poorani, S. Selvam, H.G. Prabu, P. Manisankar, J. Jeyakanthan, V.K. Langeswaran, Improved conductivity and antibacterial activity of poly(2-aminothiophenol)-silver nanocomposite against human pathogens, J. Photoch. Photobio. B 178 (2018) 323–329.
[29] A. Celebioglu, F. Topuz, Z.I. Yildiz, T. Uyar, One-step green synthesis of antibacterial silver nanoparticles embedded in electrospun cyclodextrin nanofibers, Carbohyd. Polym. 207 (2019) 471–479.
[30] M. Monerris, M. Broglia, I. Yslas, C. Barbero, C. Rivarola, Antibacterial polymeric nanocomposites synthesized by in-situ photoreduction of silver ions without additives inside biocompatible hydrogel matrices based on N-isopropylacrylamide and derivatives, Express Polym. Lett. 11 (2017) 946–962.
[31] L. Du, Y.J. Wang, K. Wang, C. Shen, G.S. Luo, In situ dispersion of oil-based Ag nanocolloids by microdroplet coalescence and their applications in SERS detection, RSC Adv. 6 (2016) 59639–59647.
[32] M.Z. Hao, W. Zhao, R.Y. Li, H. Zou, M. Tian, L.Q. Zhang, W.C. Wang, Surface modification of as-prepared silver-coated silica microspheres through mussel-inspired functionalization and its application properties in silicone rubber, Ind. Eng. Chem. Res. 57 (2018) 7486–7494.
[33] X.Z. Chen, F. Liang, W.Z. Lu, Z. Jin, Y.F. Zhao, M. Fu, High permittivity nanocomposites embedded with Ag/TiO_2 core–shell nanoparticles modified by phosphonic acid, Polymers 10 (2018) 586.
[34] P. Bihari, M. Vippola, S. Schultes, M. Praetner, A.G. Khandoga, C.A. Reichel, C. Coester, T. Tuomi, M. Rehberg, F. Krombach, Optimized dispersion of nanoparticles for biological in vitro and in vivo studies, Part. Fibre Toxicol. 5 (2008) 14.
[35] L. Du, Y.J. Wang, W.D. Zhang, C. Shen, G.S. Luo, Preparation of nonaqueous silver nanosuspensions by in situ dispersion of the surface-modified nanoparticles, Colloid. Surface. A 501 (2016) 114–121.
[36] X. Huang, D.R. Wang, L.Y. Hu, J.J. Song, Y.Q. Chen, Preparation of a novel antibacterial coating precursor and its antibacterial mechanism, Appl. Surf. Sci. 465 (2019) 478–485.
[37] M. Chen, S.X. Zhou, B. You, L.M. Wu, A novel preparation method of raspberry-like PMMA/SiO_2 hybrid microspheres, Macromolecules 38 (2005) 6411–6417.
[38] Y. Ding, Y. Chen, J.P. Zheng, Dispersion of nanoparticles in polymer matrices with well-designed ligands as dispersant/emulsifier/comonomer, Compos. Sci. Technol. 156 (2018) 215–222.
[39] M.K. Poddar, S. Sharma, V.S. Moholkar, Investigations in two-step ultrasonic synthesis of PMMA/ZnO nanocomposites by in-situ emulsion polymerization, Polymer 99 (2016) 453–469.
[40] Z.H. Chen, F. Yu, X.R. Zeng, Z.G. Zhang, Preparation, characterization and thermal properties of nanocapsules containing phase change material n-dodecanol by

miniemulsion polymerization with polymerizable emulsifier, Appl. Energ. 9 (2012) 7–12.
[41] S. Bilgin, R. Tomovska, J.M. Asua, Surfactant-free high solids content polymer dispersions, Polymer 117 (2017) 64–75.
[42] H.X. Fang, S.X. Zhou, L.M. Wu, Microphase separation behavior on the surfaces of PEG-MDI-PDMS multiblock copolymer coatings, Appl. Surf. Sci. 253 (2006) 2978–2983.
[43] S. Bai, X.H. Li, R.C. Zhang, C. Li, K.Y. Zhu, P.C. Sun, Y.H. Zhao, L.X. Ren, X.Y. Yuan, Enhancing antifogging/frost-resisting performances of amphiphilic coatings via cationic, zwitterionic or anionic polyelectrolytes, Chem. Eng. J. 357 (2019) 667–677.
[44] S.V. Patwardhan, F.S. Emami, R.J. Berry, S.E. Jones, R.R. Naik, O. Deschaume, H. Heinz, C.C. Perry, Chemistry of aqueous silica nanoparticle surfaces and the mechanism of selective peptide adsorption, J. Am. Chem. Soc. 134 (2012) 6244–6256.
[45] B.A. Bhanvase, D.V. Pinjari, P.R. Gogate, S.H. Sonawane, A.B. Pandit, Synthesis of exfoliated poly(styrene-co-methyl methacrylate)/montmorillonite nanocomposite using ultrasound assisted in situ emulsion copolymerization, Chem. Eng. J. 181 (2012) 770–778.
[46] N. Kumar, A. Mandal, Oil-in-water nanoemulsion stabilized by polymeric surfactant: characterization and properties evaluation for enhanced oil recovery, Eur. Polym. J. 109 (2018) 265–276.
[47] M. Qiu, C.J. He, Novel zwitterion-silver nanocomposite modified thin-film composite forward osmosis membrane with simultaneous improved water flux and biofouling resistance property, Appl. Surf. Sci. 455 (2018) 492–501.
[48] W. Guo, C. Yu, S.F. Li, J. Yang, Z.B. Liu, C.T. Zhao, H.W. Huang, M.D. Zhang, X.T. Han, Y.Y. Niu, J.S. Qiu, High-stacking-density, superior-roughness LDH bridged with vertically aligned graphene for high-performance asymmetric supercapacitors, Small 13 (2017) 1701288.
[49] L.H. Zhu, Y.J. Guan, Y.J. Wang, Z.D. Xie, J. Lin, J.Q. Zhai, Influence of process parameters of ultrasonic shot peening on surface roughness and hydrophilicity of pure titanium, Surf. Coat. Tech. 317 (2017) 38–53.
[50] A. Razmjou, J. Mansouri, V. Chen, The effects of mechanical and chemical modification of TiO_2 nanoparticles on the surface chemistry, structure and fouling performance of PES ultrafiltration membranes, J. Membr. Sci. 378 (2011) 73–84.
[51] C.F. Wang, M. Zhao, J. Li, J.L. Yu, S.F. Sun, S.S. Ge, X.K. Guo, F. Xie, B. Jiang, E.K. Wujcik, Y.D. Huang, N. Wang, Z.H. Guo, Silver nanoparticles/graphene oxide decorated carbon fiber synergistic reinforcement in epoxy-based composites, Polymer 131 (2017) 263–271.
[52] C. Cheng, A. He, C.X. Nie, Y. Xia, C. He, L. Ma, C.S. Zhao, One-pot cross-linked copolymerization for the construction of robust antifouling and antibacterial composite membranes, J. Mater. Chem. B 3 (2015) 4170–4180.
[53] Z.X. Voo, M. Khan, K. Narayanan, D. Seah, J.L. Hedrick, Y.Y. Yang, Antimicrobial/antifouling polycarbonate coatings: role of block copolymer architecture, Macromolecules 48 (2015) 1055–1064.
[54] M. He, Q. Wang, W.F. Zhao, C.S. Zhao, A substrate-independent ultrathin hydrogel film as an antifouling and antibacterial layer for a microfiltration membrane anchored via a layer-by-layer thiol-ene click reaction, J. Mater. Chem. B 6 (2018) 3904–3913.
[55] M. Pollini, M. Russo, A. Licciulli, A. Sannino, A. Maffezzoli, Characterization of antibacterial silver coated yarns, J. Mater. Sci.-Mater. M. 20 (2009) 2361–2366.
[56] R. Liu, L. Dai, C.L. Si, Z.G. Zeng, Antibacterial and hemostatic hydrogel via nanocomposite from cellulose nanofibers, Carbohyd. Polym. 195 (2018) 63–70.
[57] B.A. Holt, S.A. Gregory, T. Sulchek, S. Yee, M.D. Losego, Aqueous zinc compounds as residual antimicrobial agents for textiles, ACS Appl. Mater. Interfaces 10 (2018) 7709–7716.
[58] S.G. Chen, S.B. Zhang, M. Galluzzi, F. Li, X.C. Zhang, X.H. Yang, X.Y. Liu, X.H. Cai, X.L. Zhu, B. Du, J.N. Li, P. Huang, Insight into multifunctional polyester fabrics finished by one-step eco-friendly strategy, Chem. Eng. J. 358 (2019) 634–642.